Experimental assessment of the sources of regulated and unregulated nanoparticles in gasoline direct-injection engines

Michèle Bardi, Guillaume Pilla, Xavier Gautrot

Standard Article

Corresponding Author:

Michele Bardi,

IFP Energies nouvelles, 1-4 av Bois Preau Bois-Préau, 92852 Rueil-Malmaison Cedex, France ; Institut Carnot IFPEN Transports Energie.

Email: michele.bardi @ifpen.fr

Experimental assessment of the sources of regulated and unregulated nanoparticles in GDI engines

Michele Bardi[1], Guillaume Pilla[1], Xavier Gautrot[1]

[1] IFP Energies nouvelles 1-4 av Bois Preau Bois-Préau, 92852 Rueil-Malmaison Cedex – France ; Institut Carnot IFPEN Transports Energie.

Abstract

This work investigates nanoparticles formation process in light-duty GDI engines operated in homogeneous combustion. The analysis specifically focuses on the contribution of particles in the range of 10-23nm, which are expected to be taken into account in future emission regulations.

Experiments were carried out on a single cylinder 0.4l displacement GDI optical engine. Exhaust gases were analysed by means of a commercial device (DMS500) to obtain a quantitative measurement of the particulates number and size. Optical diagnostics (broadband color imaging and liquid phase LIF) were employed to correlate the exhaust measurements to the in-cylinder physical phenomena. The main leverages to control soot particulates formation were investigated.

The engine temperature was found to have a significant impact during the entire warm-up phase on the global particulates number (PN) and also on the relative contribution of the 10-23nm range to the total PN. Injection phasing has also a primary role in the formation of particulates in the small range of the spectrum when operating in mild stratified combustion mode. On the other hand, an increased in-cylinder aerodynamic (e.g. combined swirl-tumble motion) has a positive impact in reducing global particulates number but also causes an increase of the 10-23nm relative contribution.

Optical diagnostics helped establishing a relationship between the detection of liquid film, the consequent pool fires and the exhaust gas measurements. The evaporation of the liquid film detected on the injector nozzle and the intake valve right after the injection appears to be decisive for the formation of nanoparticles in pool fire mode. The experimental results indicate that when pool fires were detected the PN increased

drastically in the whole range of the spectrum including the 10-23nm range. Authors relate this effect to in-homogeneities in the fuel mixing field induced by the evaporation of the liquid film.

Introduction

To increase the performances and simultaneously reduce the fuel consumption of spark ignited (SI) engines the introduction of fuel in the cylinder evolved to direct injection strategy. This technology allows cooling the charge thus helping downsizing and compression ratio increase. While greatly improving the engine efficiency, particulates emission emerged as a new significant issue [1–4]. Therefore during the past few years worldwide emissions regulation were introduced to decrease particulates number (PN) and mass (PM) produced by spark ignited (SI) engines. Hence EURO VI in EU set a PM/PN limit to 4.5mg/km and $6x10^{11}$part/km respectively [5]. To take into account the sensitivity of measurement procedures and prevent measurements errors, the current regulations exclude the smallest particulates, below 23nm. Nevertheless the size distribution in gasoline direct injection (GDI) engines may be wide due to higher concentration of volatiles in the fuel. Proportion of sub-23nm particulates reported in the literature is up to 40% [6,7]. Since it is well known that the smaller the particulates, the more harmful they are [8], and considering the improvement in nanoparticles measurement protocols [9], an evolution of the regulations towards sub-23nm particulates can be expected.

The mechanisms of formation of particulates in gasoline engine have been extensively studied in the literature. The specificity of GDI technology degrades mixture preparation, compared to port fuel (PF) injection, which is one of the major causes of particulates formation [10–12]. This phenomenon will contribute to vapor fuel stratification, liquid film on the combustion chamber walls and residual droplets during combustion development. Hence the formation of particulates takes its origins in two different combustion phenomena: diffusive burning of liquid fuel – pool fires and droplets, and homogeneous gas-phase combustion of locally rich zone, both of which strongly contribute to particulates formation. In relation with these physical phenomena, engine control parameters and combustion parameters will affect their formation. Among these parameters, wall temperature, injection phasing and aerodynamics are within the most significant [13]. Wall temperature will directly govern the liquid film formation and evaporation and thus the pool fires occurrence. Injection phasing will play a role in liquid films formation through wall impingement and also in rich gaseous combustion through mixing duration. Finally aerodynamics will play a role in the fuel evaporation, and thus the homogeneity of the mixture in the chamber.

This paper aims at investigating the mechanisms responsible for particulates formation, with a specific focus on the 10-23nm range contribution to the total particulates emission. The overall goal of this work is to provide understanding and experimental data to accompany technological development and modeling validation. To conduct this study a direct injection optical single cylinder engine was operated and dedicated instrumentation was deployed. A reference test condition representative of a part-load point (0.45 MPa x 1200 rpm) has been investigated including a number of parametric variations (e.g. engine temperature, injection pressure and phasing). The understanding achieved in this paper is based on the combination of two experimental approaches: exhaust gas analysis by means of a differential mobility spectrometer (DMS) which provides a quantitative measurement of the PM and PN resulting from the combustion process; and in cylinder optical diagnostics, including high speed broadband color imaging and liquid laser induced fluorescence (LIF) both of which enable a qualitative understanding of the phenomena taking place before and during the combustion.

Material and methods

The single cylinder optical engine

Experiments were performed on a 0.4 l displacement, single-cylinder engine and the main features are described in Fig. 1 together with a schematic presentation of optical accesses and injector targeting.
The engine is designed to have a flexible configuration providing different optical accesses to the combustion chamber:

- Piston optical access: an extended (Bowditch) piston equipped with a 45° mirror enables the optical access through the piston sapphire window;
- Cylinder optical access: a 30 mm high sapphire cylindrical insert is located in the upper part of the cylinder to provide a lateral view on the combustion chamber during the compression and expansion strokes
- Engine head window: two line-of-sight optical accesses are placed on the opposite sides of the engine head to provide a view of the combustion chamber at TDC

Two injection systems are installed and the engine can be switched from port to direct fuel injection system. The GDI injector is a Bosch HDEV-5 injector equipped with a 6-orifice nozzle each one featuring a counter bore to foster jet mixing. The nozzle permeability is 303 cm^3/30s and considering a discharge coefficient C_d = 0.85 the resulting average orifice diameter is 114 µm. The injector is mounted centrally in the combustion chamber with a slight angle between the cylinder and injector axis (7 °, c.f. Fig. 1) while the average included angle of the jets is 60°. Finally, the fuel used is Euro 6 standard E10 gasoline.

Engine displacement:	0.4 l
Volumetric compression ratio:	10.5:1
Bore x Stroke (mm):	77 x 86
Number of intake /exhaust valves:	2
Valve timing (CAD aTDC):	IVO 10 IVC 210 EVO -220 EVC -10
Injection system:	DI / PF
DI injector	Bosch HDV 6 6 holes
Injection pressure (MPa)	20

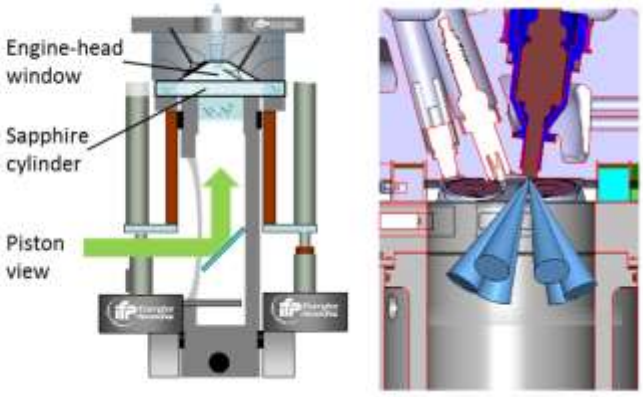

Fig. 1 Single cylinder cylinder optical engine description. Main features (left), optical accesses (center) and injector targeting (right).

Valve timing is set in order to have a slight negative valve overlap, with the aim of having a better control on the total air trapped mass.
The piston rings, specifically designed for the optical engine, are composed of a graphite based material. Therefore, they are self-lubricating and the combustion chamber is oil-free. Despite being less representative of a real engine, this fact has two advantages: it prevents lubricant oil to deposit on optical access surfaces, keeping them clean for longer periods, and it helps focusing the study on the particulates formation processes which are linked to fuel related processes (liquid film evaporation, air fuel mixing).

A lambda sensor was used to measure oxygen content in the exhaust and to set the fuel injection duration to achieve the mixture stoichiometry required for the test at a constant inlet air flow rate.

Particulates sizing

In addition to standard measurement systems, such as gas analysis test bed (CO2, CO, O2, NOx and HC), particulates emissions were measured using a Differential Mobility Spectrometer, Cambustion DMS 500 [14]. Sampling was performed with a beveled tube placed in the middle of the exhaust line at approximately 1 m from the exhaust port. The particle count is performed automatically by the Cambustion software and the sample dilution, operated directly by the device, is varied following the software indication to have the best signal to noise ratio during each measurement, by preserving electrometer from to high PN concentration. The dilution rate is varied between 5 and 100.
The nominal particulate size range detected by the device is 5-1000nm. However, after a comprehensive analysis of the results only the 10- 230nm range is kept. As shown in Fig. 2, the sub-10nm range measurements appeared extremely unstable and the values measured were neither repeatable nor coherent with the engine conditions.
On the other hand, the over-230nm range was not considered because for all the cases tested the value was comparable to the noise level.
Being the objective of the paper to understand the 10-23nm range particles emission and their contribution to the total PN, a specific analysis of the spectrometer results has been carried out calculating the two following parameters: PN_{tot} as the total particle count in the 10-230nm range and $PN_{10\text{-}23}$ the particle count in the 10-23 nm range. Finally, the relative contribution of the 10-23nm particulates (PN_{ratio}) is obtained as:

$$PN_{ratio} = \frac{PN_{10-23}}{PN_{tot}} \qquad (1)$$

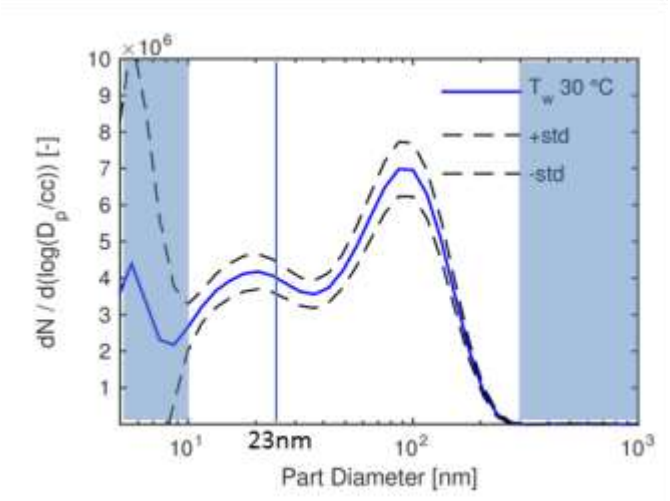

Fig. 2: Sample DMS results in linear scale. The standard deviation obtained over a single test at stabilized conditions is indicated in dashed line (60 s). The blue areas indicated the ranges not accounted for the PN_{tot} and $PN_{10\text{-}23}$ counts.

Also, to validate the consistency of the measurements, tests have been performed by repeating the engine operating point several times (on different days, before and after cleaning the

measurement system). Also, the time variability of the particle-size spectra was analyzed by excluding not stable measurements and the resulting spectra was calculated as a robust average excluding the 10% from each end of the data by considering the instantaneous PN_{tot}.

In cylinder measurements

Optical diagnostics were put in place to establish a relationship between exhaust measurements and in-cylinder processes.

Broadband color imaging

A Photron AX100 high-speed color camera was employed for a global observation of the in-cylinder processes [13]. The images captured enable a clear distinction between the chemiluminescence produced during the premixed combustion (blue color) and the yellow-orange luminous emissions related to the incandescence of soot formed in pool fires [15]. The camera was placed in different positions to better locate the soot formation in the combustion chamber volume: in particular, the combustion chamber was visualized alternatively through the transparent cylinder or the piston window. The camera frame rate was set to 10kHz corresponding to 1 image every 0.7 °CA.

Liquid Phase Laser induced fluorescence (LIF)

Different techniques are available to have quantitative measurements of liquid film formation in the combustion chamber such as refractive index matching [16] or infrared radiation [17]. However, the objective of this study is to identify *where* the liquid film is formed rather than its quantification. Laser induced fluorescence (LIF) was chosen to investigate the formation of fuel liquid films on the cylinder head and on the piston [18,13]. The optical layout is schematically presented in Fig. 3.
A diverging laser beam was set to illuminate most of the combustion chamber volume, including the piston surface and most of the cylinder head. The fluorescent signal was captured using an intensified camera (Princeton PiMAX) and a band-pass filter to reject the flame broadband emissions and laser beam reflections (450nm±10).

An excitation wavelength of 355nm (third harmonic of a Nd:YAG laser) was preferred to the more commonly used 266nm wavelength. Many species present in commercial fuels (e.g. aromatic hydrocarbons) have a strong fluorescent signal when excited at 266nm.As a consequence light absorption from fuel both liquid and vapor phase would be too high making it difficult to illuminate correctly the cylinder head after the end of injection. On the contrary, when excited at 355nm, commercial gasoline is almost transparent and no fluorescent signal can be detected. In this case, the addition of a small amount of a fluorescent tracer (TMPD at 0.1%) was added to the fuel. This small concentration assures to have detectable signal from the fuel in very high concentration (e.g. in liquid phase) and simultaneously a negligible absorption, and thus parasitic fluorescent emission, from the vapor phase [19].

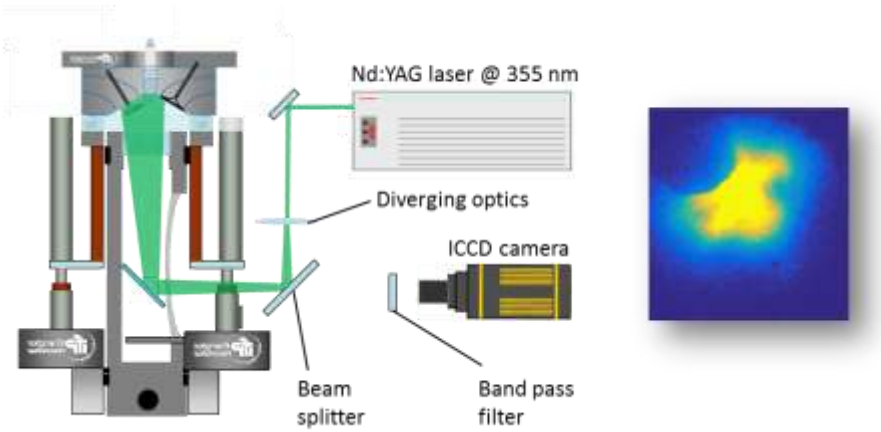

Fig. 3: Optical layout for liquid fuel film visualization.

The camera lens was set to obtain a wide depth of focus reducing the diaphragm aperture: acceptable image sharpness was obtained on a wide range of distances including the cylinder head and the piston surface at BDC.
TMPD boiling temperature is 260 °C: Considering the distillation curve of a commercial gasoline and the strong co-evaporation effects linked to the small tracer percentage used (0.1 %), the tracer is considered to evaporate together with the heaviest fractions of the fuel [20,20,21]. Considering the low amount of tracer employed, it is not considered to have an impact on physic chemical characteristics of the fuel.

Working conditions and test plan

A single operating condition representative of a medium/low load – low speed operating point was investigated: 0.45MPa indicated mean effective pressure (IMEP) at 1200rpm. This operating point can be considered representative of cold start or take-off phase, which are predominant in urban usage. The spark advance was regulated to keep the CA50 at 7° *aTDC*, while the global equivalence ratio was fixed at the unit (stoichiometric) with no EGR dilution. A *EURO6* standard gasoline fuel containing 10% ethanol was used. The gas temperature and pressure at IVC (intake valve closing) at reference condition is respectively 40°C and 0.541 bar. While the intake temperature has been kept constant, the intake pressure has been adjusted to keep the IMEP constant especially when in cylinder aerodynamics has been modified.
Parametric variations to the reference condition (e.g. coolant temperature, injection phasing and aerodynamics) were applied to understand the impact on the particulate emissions. All the acquisitions were carried out at stabilized engine conditions.
The parametric variations applied are detailed below:

Coolant temperature: coolant water temperature has been modified starting from temperatures typical of steady warm-engine conditions (T_w 85 °C) to temperatures more relevant to warm-up phase operations (T_w 30 °C). The coolant temperature has a significant impact on the combustion chamber wall temperature. However, it is important to remind that the engine is operated in steady conditions meaning that the surface temperatures are expected to be significantly higher than the water temperature. Nevertheless this variation helped to understand how the wall temperature affects liquid film evaporation and particle formation.

Injection phasing: several single injection strategies have been tested by modifying the phasing of the start of injection (SOI) from 360 to 60 CAD bTDC. This variation allowed to investigate different combustion modes including fully homogeneous to highly-stratified cases.

Aerodynamic: three different configurations have been tested to modify the in-cylinder air motion, by the introduction of aerodynamic elements in the intake port and the alteration of the valve control. In details:

1. *Reference Tumble*: the tumble motion is obtained by the shape of the intake duct,
2. *Increased tumble*: an aerodynamic insert is placed within the intake duct to redirect the air flow and to increase the tumble motion by approximately 20%.
3. *Swumble*: an aerodynamic insert is added, as in the previous configuration, and the valve lift is modified: in *Swumble* mode one of the two intake valves is deactivated. In this way, the asymmetric intake flow combines the *tumble* and the *swirl* motion (hence the name *Swumble*) [22,23].

For the *increased tumble* and for the *swumble case* to assist the increased kinetic energy is slightly increased to a maximum of 0.564 bar.
The parametric variations tested are summarized in Table 1.

Table 1: Summary of the parametric variations carried out in the experimental test campaign.

Parameter	Values
Tw (°C)	30 - 40 -60 - 85
SOI (CAD bTDC)	360 -… - **260** -… - 60 @Tw 85 °C **260** - 180 @Tw30°C
Aerodynamic configuration	**Ref Tumble** - Increased tumble - Swumble

Results

In this section the DMS results are presented together with the results obtained by means of the optical diagnostics.

Measurement precision and noise level

Figure 4 presents the results obtained for different coolant temperatures settings operating the engine in GDI mode with an early injection (SOI 260 CAD bTDC) . The detected PN spans over different order of magnitudes when modifying ambient temperature. The measurement standard deviation presented in Fig. 4 on a logarithmic scale highlights how this parameter has a different relative impact depending on the PN sampled. While at low temperature the standard deviation is almost negligible in the 10-230nm particulates size range, for T_w = 85 °C it becomes of the same order of magnitude of the average value itself.
A test has been performed operating the engine in port fuel mode with the objective of having a reference of a completely homogeneous combustion. The comparison between the PF case and the reference GDI case does not show any statistically relevant difference: the mixing field for the reference case is therefore expected to be homogeneous.
Since for the PF case the PN emission is expected to be negligible, this measurement will be used as a reference for the DMS noise level, and only higher values will be considered reliable.

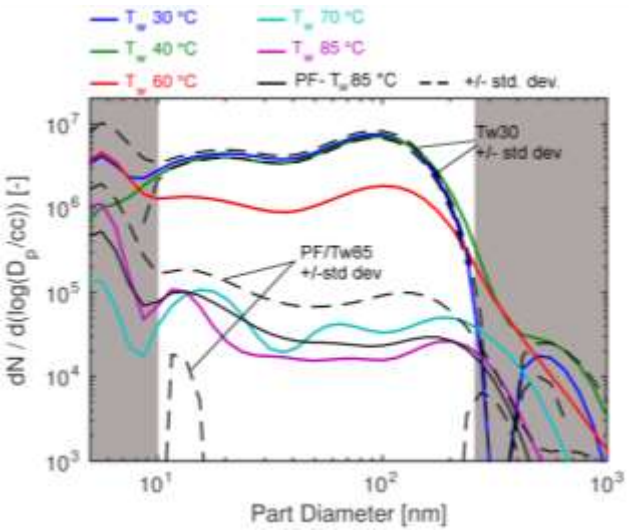

Fig. 4: Effect of T_w on particulate emissions. The part of the spectrum not considered for the analysis is indicated by the gray areas. The measurement obtained in port-fuel injection mode is plotted in solid black line for reference.

Effect of coolant temperature

No statistically relevant difference can be observed between the GDI and the PF case at T_W 85°C: despite the interaction between the spray and the intake valve the fuel is evaporating to completion and the tumble motion is making the gas mixture homogeneous.
On the contrary, when the coolant temperature is decreased, the number of particulates detected increases substantially on the entire range measured. However, the effect of the coolant temperature is observable at T_w 30 °C and 40 °C (as expected) but also at T_w 60 °C. This means that the entire warm up phase is critical for PN_{tot} emission.
Fig. 5 summarized the results presented in Fig. 4 displaying the corresponding PN_{tot} and PN_{ratio} values. The plot underlines the high sensitivity of PN to the coolant temperature indicating an increase of almost two orders of magnitude when reducing T_w from 85 °C to 60 °C. On the other hand the plots indicate that for all the cases there is a substantial contribution of the 10-23nm range with PN_{ratio} = 0.25 for T_w = 30 °C increasing progressively to 0.55 for the reference condition (T_w = 85 °C).

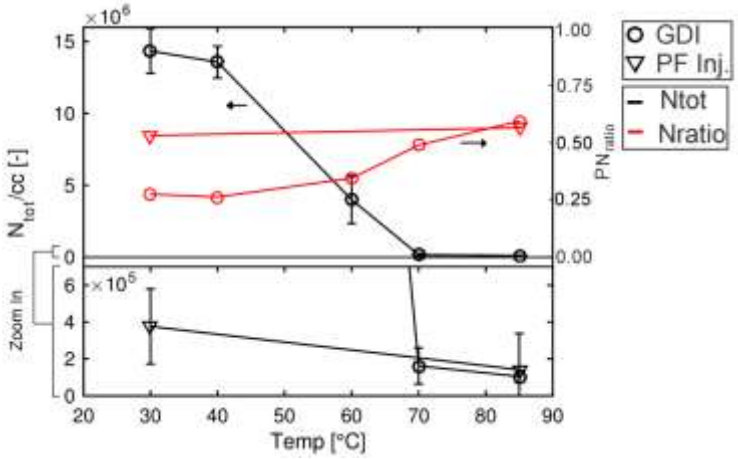

Fig. 5: Effect of Tw on PNtot , (in black, on the left y-axis) and PNratio, (in red, on the right y-axis). The standard deviation is presented together with the PNtot values. For GDI cases, SOI 260 CAD bTDC.

High-speed color imaging has been employed to investigate the causes for soot formation. Fig. 6 presents images of the combustion chamber captured from the piston window during the combustion (15 CAD aTDC). In Broadband color images different phenomena can be identified: the region where chemical reactions take place characterized by a light blue color; the regions where soot formed in pool fire mode, by the yellow orange emissions typical of soot incandescence for these range of temperatures (red circles in Fig. 6). In the images, can be also distinguished yellow-green emissions that have been observed for all the conditions tested including in the reference noise case (port fuel - warm engine; white circles in Fig. 6). Although it is not possible to clarify completely the issues, authors believe it is related to the wear of the piston rings employed in the optical engine. Despite the visual appearance a relationship between the emissions observed and the exhaust measurement has not been found, and therefore their effect is neglected.

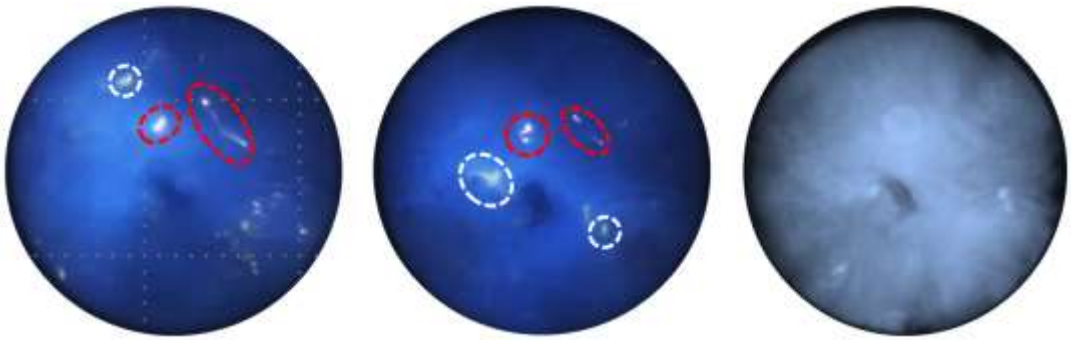

Fig. 6: Broadband color images for different engine temperatures taken at 15 CAD aTDC. Tw 30 °C (left), Tw 60 °C (center) and Tw 85 °C (right). Soot formed in pool fires mode can be observed in the images (red circles).

Soot incandescence originated by pool fires can be clearly identified for the cases at T_w = 30 °C and T_w = 60 °C. For the two cases, soot emissions seem to originate from different regions: in particular around the intake valve seat and the injector nozzle tip. The consistent observation of this phenomenon over several cycles and the specific location where soot is observed suggest a pool fire combustion mode as consequence of a liquid fuel film. Also, soot incandescence can be

observed on the lower-right part of the image (only for T_w 30 C). In this case the observation of these phenomena is not repeatable in intensity and in location (hence it is not visible in Fig. 6).
In order to verify the hypothesis of liquid fuel formation Fig. 7 presents a time sequence of liquid film LIF obtained for two different coolant temperatures (T_w = 30 °C and 85 °C). In the reference case, LIF signal from liquid fuel can be observed only shortly after the end of the injection (250 CAD bTDC). After that, the fuel evaporates quickly and no signal is detected. On the other side, when coolant temperature is decreased, liquid films can be clearly distinguished on the valve seat and on the injector nozzle. These results are consistent with the soot incandescence observed in Fig. 6. The particles are formed in pool fire mode due to the combustion of the liquid film observed in Fig. 7. The liquid film on the valve seat is formed during the injection, where the intake valve is still open.

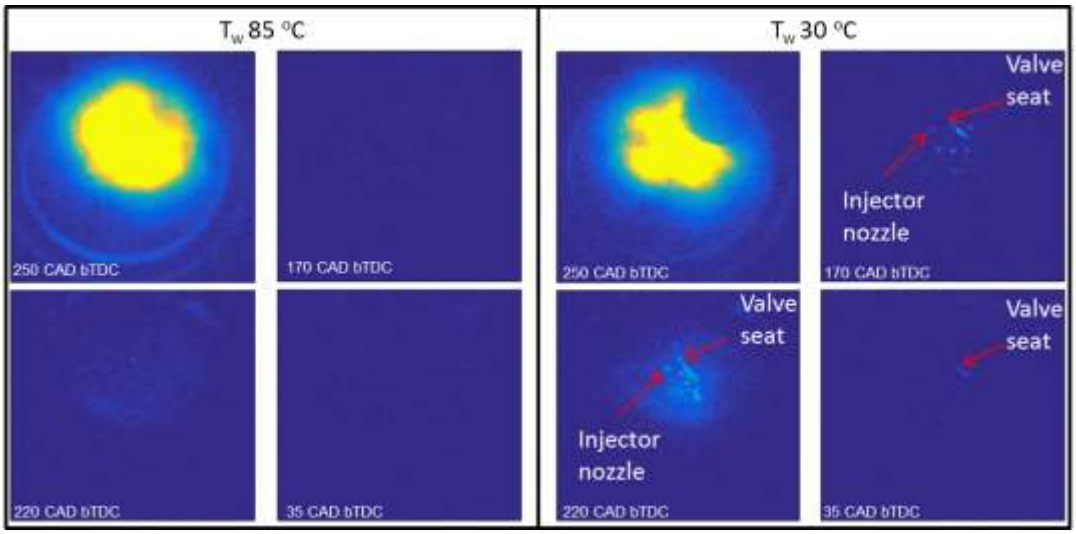

Fig. 7: Liquid fuel film detection. LIF signal for T_w 85 °C (left), and T_w 30 °C (right). SOI 260 CAD bTDC.

While for the reference case the higher temperature of the valve leads to its fast evaporation, for lower temperatures the liquid film remains until the combustion starts: despite the images cannot indicate exactly the moment when the liquid film evaporates completely, due to a sensitivity issue, the liquid film is still visible on the valve seat at 35 CAD bTDC. Coolant temperature also affects the liquid film evaporation on the injector nozzle. As shown by [24] at ambient temperature and pressure, injector nozzle wetting can be a significant issues for nozzles featuring counter-bored orifices, as in the present study. The images in Fig. 7 test confirm that in the present case injector wetting causes the persistence of a fuel liquid film on the nozzle during the compression stroke: also in this case, the lower temperature of the coolant is causing a slower evaporation of the liquid film leading eventually to a pool fire.
The interpretation of the pool fires observed in the lower-right part of the T_w 30 °C case in Fig. 6 is more difficult. Some insight can be found in the LIF images presented in Fig. 7: apart from the liquid films observed on the valve seat and injector nozzle, which appear consistently at the same place, there are other emitting sources which appear in erratic location. In author understanding, this LIF signal can be related to coalescent droplets, formed after the interaction of the spray and the intake valve which eventually reach the piston forming a liquid film: this would explain the pool fires observed previously.
In summary, a reduction in T_w causes liquid film to form and persist on i) the intake valve seat, due to the valve-spray interaction during the injection, ii) the injector nozzle and iii) the piston surface, as a consequence of droplet coalescence after the injection spray interaction. Liquid film formation results in pool fires at the corresponding location. The observation of pool-fires in the

combustion chamber is related to a significant increase of PN_{tot} in the exhaust. Despite a reduction of PN_{ratio} when reducing T_w, which can be related to predominance pool-fire combustion mode, the contribution of PN_{10-23} is always > 25%. This means that the formation of liquid films strongly affects soot formation in the accumulation mode but also in the nucleation mode. An open question is if the nucleation particles are produced in the area where pool fires are observed, or further downstream as a consequence of the heterogeneities caused by the liquid film evaporation.

Injection phasing

In this section the effect of injection phasing on soot formation is discussed presenting separately the results obtained for reference and cold engine conditions (T_w 30 °C).

Injection phasing – warm engine

The left-hand side plot of Fig. 8 displays results obtained at warm engine conditions: as discussed in the previous section, for the reference case the PN_{tot} measured is below the noise limit (PN_{tot} measured for the PF case). Modifying the SOI among a wide range (220 – 360 CAD bTDC) does not have any detectable effect on PN_{tot} measurement. This observation suggests that, despite the spray impingement on the piston surface (e.g. for SOI 360 bTDC) and on the intake valve, the surface temperatures prevents liquid film formation.

The important difference observed in the formation of liquid films on the valve seat and on the piston might be related to a change of regime of the liquid film evaporation: for T_w 85°C it is possible the surface temperature exceeds Leidenfrost temperature causing the regime to switch to film boiling. As shown in [25] this boiling regime strongly reduces the surface wetting and therefor restricts liquid film significance.
At the same time, the PN_{ratio} measured for these conditions cannot be considered reliable due to the uncertainty of the measurements.
When injection phasing is further advanced (SOI <200 CAD bTDC), PN_{tot} exceeds the noise limit: if PN_{tot} remains at relatively low values for SOI< 90 CAD bTDC a dramatic increase is observed for SOI = 60 bTDC.

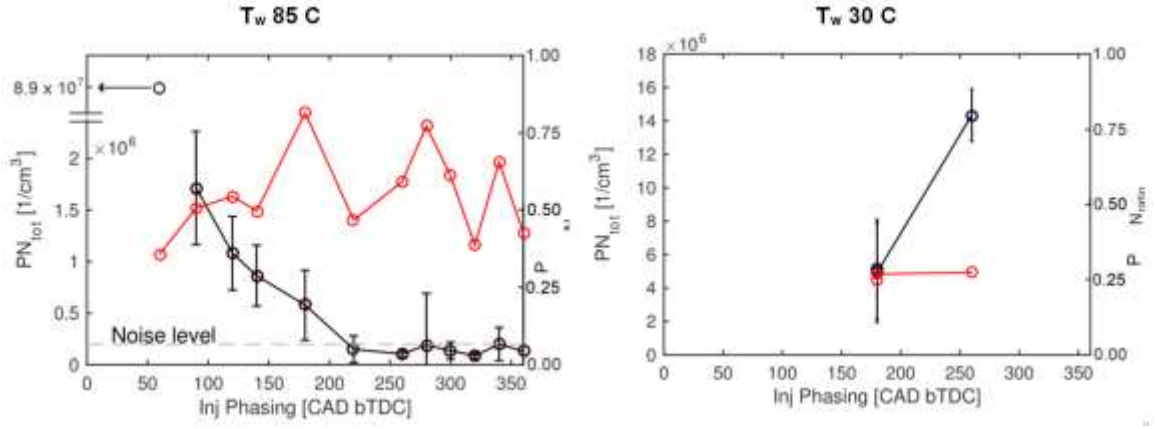

Fig. 8: Effect of injection phasing on PNtot, (in black, on the left y-axis) and PNratio, (in red, on the right y-axis). The standard deviation is presented together with the PNtot values.

The maximum PN_{ratio} is measured for SOI = 180 CAD bTDC, and it decreases progressively for shorter injection advances however the values remain significantly high (~0.5).

As expected, when the fuel is injected later, the time available for the spray to mix with in cylinder gases decreases and, as a consequence of that, at the time of the ignition the fuel distribution is less homogeneous. However, broadband images in Fig. 9 give further insights about soot formation mechanisms at these conditions. Upper left image refers to the reference case, but an identical scenario has been observed for all the cases until SOI = 180 CAD bTDC (included). In consistency with DMS measurements, no soot incandescence is detected in the combustion chamber. On the other images (SOI < 140 CAD bTDC) soot incandescence can be clearly detected around the injector nozzle: this fact is associated to the liquid film around the nozzle tip (injector wetting [24]), which has not enough time to evaporate for late injections. This means that at these conditions, apart from mixing in-homogeneities, injector wetting is an additional cause of soot formation. On the other hand, for SOI 60 CAD bTDC soot incandescence can be observed on the injector tip and on the left side of the combustion chamber. As observed in [11], when the piston is very close to the injector at the moment of the injection, the fuel droplets impact the piston at high velocity. This can results in droplet bouncing and consequent impact on the cylinder walls, resulting in a further pool fire.
PN_{ratio} is significantly higher when compared to the values obtained at lower coolant temperature cases. This observation suggests that, despite liquid films evaporate faster than for the cold engine case, the evaporated fuel might not mix properly to reduce local equivalent ratio and to avoid soot formation. On the other hand, with the data available in this paper it is not possible to distinguish if the stratification causing soot formation is due to the spray gas mixing or, for example, to in-homogeneities related to the evaporation of the liquid films (e.g. on the injector nozzle).
The case SOI = 180 CAD bTDC is interesting because on the images no pool fires have been observed while PN_{tot} appears above the noise level. Considering the consistency of this result, verified by repeating the measurement several times (e.g. on different days), authors believes that soot incandescence is too low to be detected by the camera. Also, in this case the liquid film on the injector might be already completely evaporated when the combustion takes place. However, this late evaporation might cause heterogeneities in the gas phase eventually resulting in soot formation. However, this interpretation needs to be corroborated by CFD simulation also considering the limitation of the DMS500 accuracy.

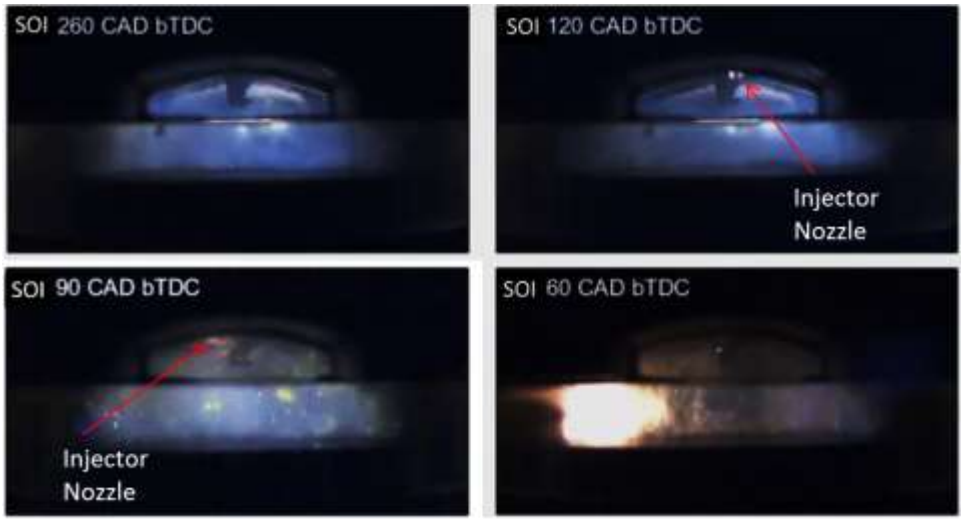

Fig. 9: Effect of injection phasing. Broad band color images at 30 CAD aTDC.

Injection phasing – cold engine

On the right hand side plot of Fig. 8, the effect of a variation in the injection phasing is tested for T_w = 30 °C. For low coolant temperatures controlling liquid fuel film formation/evaporation is critical to avoid pool fires. In this case, injecting at SOI = 180 CAD bTDC is beneficial for reducing

PN emissions because the spray-valve interaction is avoided. Also, being the piston further from the injector tip than in the other case, there is less possibility of formation of liquid deposits on the piston surface.
LIF images (Fig. 10) confirm this aspect: the only detectable LIF signal is detected around the injector tip. The results indicate that avoiding the spray-valve and piston interaction significantly improves in cylinder mixing. The similar PN_{ratio} value suggests that for both cases soot is formed in similar combustion mode (pool fire).

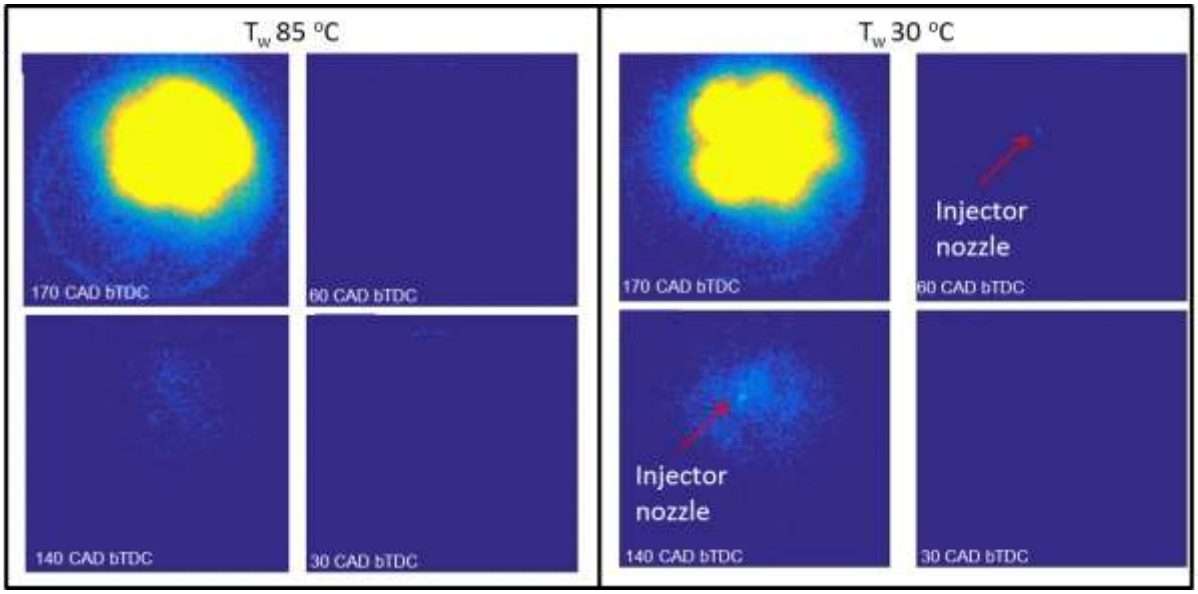

Fig. 10: Liquid fuel film detection. LIF signal for T_w 85 °C (left), and T_w 30 °C (right). SOI 180 CAD bTDC.

In-cylinder aerodynamics

As previously showed, during the engine warm up phase (T_w < 60 °C) liquid film formation and pool fires were identified as responsible for important PN emissions.
Fig. 11 presents the impact of in-cylinder aerodynamics at cold engine conditions (T_w = 30 °C) on PN_{tot} and PN_{ratio}.
The two injection phasing discussed in the previous section were tested to understand the effect of aerodynamics with and without valve impingement. For both cases, increasing in-cylinder aerodynamics is beneficial for reducing particulates formed in the entire size range. In particular, *swumble* motion enables a PN_{tot} reduction of 95% and 70% for SOI 260 and 180 CAD bTDC respectively. As discussed in section 2.4, *swumble* motion is achieved by deactivating one of the two intake valves, and more precisely, the one interacting with the spray. This result confirms at the same time the advantage of implementing this advanced air motion and the negative effect of the spray-valve interaction on particulates emissions. Also, swumble motion is the only case for which PN_{tot} is lower for SOI 260 CAD bTDC: in this case, since valve impingement is avoided, the advantage of the earlier injection is reflected in a more complete fuel air mixing and therefore less particulates emissions. Increased aerodynamics causes only a weak increase on PN_{ratio} meaning that, in absolute value, $PN_{10\text{-}23}$ is reduced.
LIF imaging was performed to understand the effect of the evaporation of the liquid fuel films on pool fires. To summarize the information, the amount of liquid fuel has been measured from each image qualitatively, by calculating the 99 percentile of the LIF detected signal and the results are shown in Fig. 12.

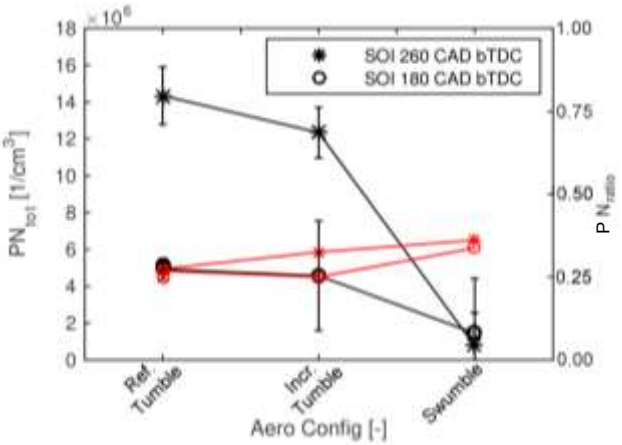

Fig. 11: Effect of in-cylinder aerodynamics on PN_{tot}, (in black, on the left y-axis) and PN_{ratio}, (in red, on the right y-axis). The standard deviation is presented together with the PN_{tot} values. T_w = 30 C.

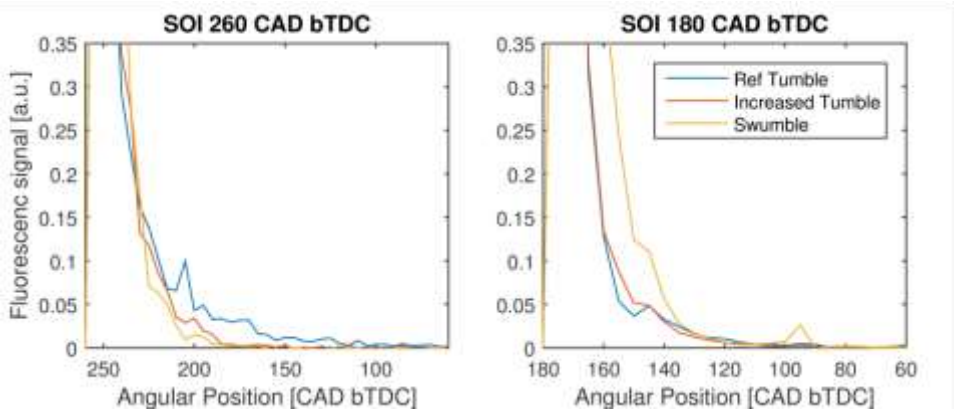

Fig. 12: Effect of in-cylinder aerodynamics. Maximum LIF signal for two different injection phasing: SOI 260 CAD bTDC (left hand side) and SOI 180 CAD bTDC (right hand side).

Results obtained for SOI 260 CAD bTDC indicate the significant effect of aerodynamics on the evaporation of the liquid film: as expected, *swumble* case presents the lowest LIF signal due to the absence of liquid film on the intake valve seat. When comparing the two tumble cases, the LIF signal decreases more rapidly for the increased tumble case. This measurement supports the idea that increased aerodynamics help reducing particulates emissions for two reasons: it improves air-fuel mixing and it fosters liquid film evaporation.

In the second case presented in Fig. 12, the same comparison is drawn for SOI 180 CAD bTDC. Due to the small area related to the injector nozzle film related to the injector wetting (the only one detected in this case, cf Fig. 10) it is more difficult to assess the differences in the three cases (e.g. no difference is observed for the *tumble* cases). However, it is interesting to observe a slower decay of the signal for the *swumble* case: a possible hypothesis is that even though air motion is stronger globally in the chamber, *swumble* motion might not be effective in the injector nozzle region, paced close to the canter of the chamber on the top of the cylinder head. In this particular region the flow velocities associated to the swirl motion are expected to be almost negligible. Another possible interpretation is that, considering the low included angle of the injection, the swumble motion might cause more plume to plume interaction and, therefore, delay

the spray evaporation. CFD flow simulations are identified as future works to better understand this phenomenon.
A further experiment was performed at warm engine conditions to investigate the impact of swumble at warm engine conditions at two different injection phasing. On Fig. 13, the results obtained for the swumble case are plotted together with the reference tumble results for comparison. While at SOI 260 CAD bTDC no significant difference can be observed (both measurements are below the noise limit) at SOI 180 CAD bTDC the reference exceeds clarly the noise limit (cf Fig. 8) but in *Swumble* case no increase in particle formation is observed.

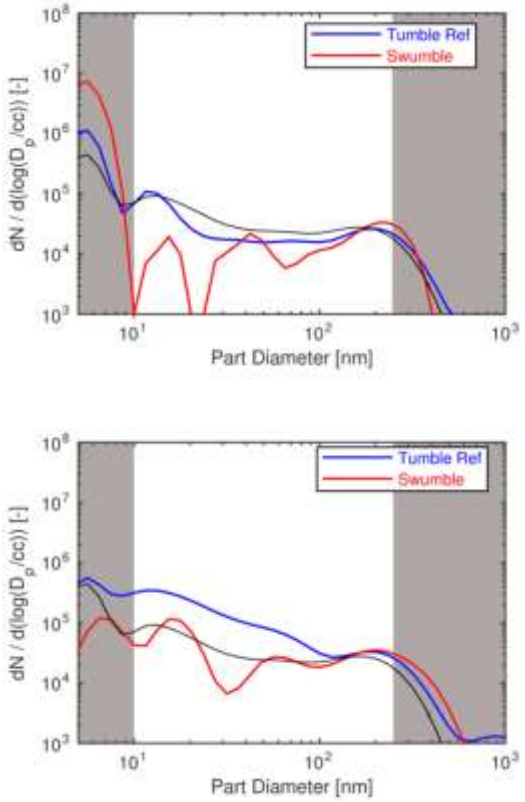

Fig. 13: Effect of in-cylinder aerodynamics on particulate emissions at two different injection phasing: SOI 260 CAD bTDC (left) and SOI 180 CAD bTDC (right). The part of the spectrum not considered for the analysis is indicated by the gray areas. The black line indicates the noise reference (PF injection case).

This comparison underline that swumble motion has a positive effect in reducing mixture stratification an prevent particulate formation. The observation of the spectra also indicates that increasing the in-cylinder motion helps reducing particulate emissions in the whole range but more specifically spectrum including the 10-23nm range.

TEM sampling

To have direct observation of soot particulates, soot has been directly sampled within the cylinder. Specific inserts were designed to host TEM grids where soot particulates are captured due to thermophoresis [26]. A sketch of the layout is shown in Fig. 14. In this configuration, the engine was operated at the reference condition for a relatively short duration (60s) to make sure to capture enough particles and afterwards the grids have been observed in a transmission

electron microscope. Two sample images are presented as a preliminary analysis result while statistical analysis will be performed in future works.

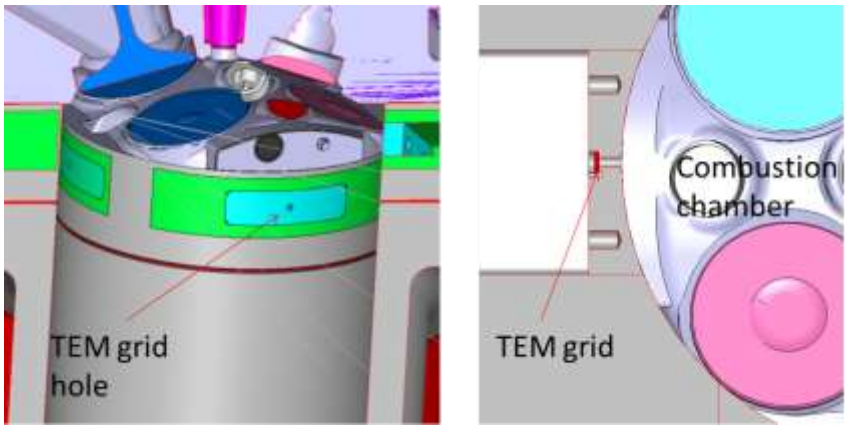

Fig. 14: TEM sampling. Schema presenting the position of the TEM grids within the cylinder.

Soot particulates collected from the grids can be observed on the two sample images presented in Fig. 15. The grid, placed on the cylinder walls.
Images show soot sampled at two different injections phasing for warm engine conditions: a homogeneous and a highly stratified case. Both images show a high number of primary particles not aggregated with a diameter falling in the range of 10-30 nm. Also the particles sampled in the highly stratified case shows a higher presence of large aggregates. More statistical analysis will be performed on the samples available to extract information about soot morphology (e.g. gyration radius, fractal dimension).

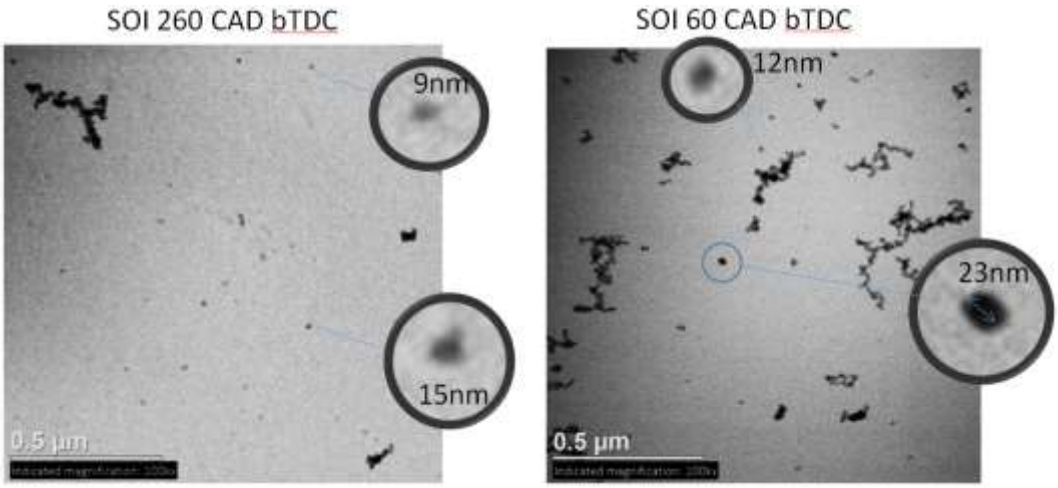

Fig. 15: TEM images obtained placing the TEM grid along the cylinder wall obtained at T_w 85 C for two different injection phasing: SOI 260 CAD bTDC (left) and SOI 60 bTDC (right).

Conclusions

This paper investigated the mechanisms behind nanoparticle formation in GDI engines and the contribution of the particles in the 10-23nm range which will be taken into account in future engine regulations.
Despite the measuring methodology might include artifacts related to the measurement device and to the volatile fraction which could also be included in the sampling, the consistency of the results obtained suggest the reliability and the relevance of the data obtained for technological development.
For all the cases tested, particulates in the 10-23nm range constitute 20 to 70% of the total particulates number. Their relative decreases at low engine temperature, and more in general when pool fires are clearly detected in the chamber during the expansion stroke.

As expected, decreasing the engine coolant temperature causes a substantial increase in PN on the whole range of the measured spectrum. The main mechanisms identified in this case are pool fires observed in different locations of the chamber: along the intake valve seat, on the injector nozzle and on the piston surface. LIF images confirmed the formation of liquid film on the valve seat and the injector nozzle.

Injection phasing effect has been observed: for warm engine conditions no particulates emission has been detected when injecting before BDC: in these conditions liquid films are not formed or evaporate soon enough to prevent soot formation and the exhaust PN measurements are hence comparable to the ones obtained for port fuel injection. On the other hand, injecting after BDC causes an increase in PN as a consequence of the progressive stratification of the charge and a pool fire develops around the injector nozzle.

Enhanced in-cylinder aerodynamics show a strong impact in reducing particulate emissions. Results showed that increasing air motion is beneficial in improving the air-fuel mixing and in reducing the time needed for liquid film evaporation. The combination of tumble and swirl motion (*swumble*) seems the most effective to reduce PN emissions. The benefits obtained thanks to enhanced aerodynamics are observed on the entire range of the spectrum including the 10-23nm range.

In general, all the observations put in evidence that in GDI engine the evaporation of the liquid films is pivotal for the reduction of particulates: apart from changing the combustion mode it is considered to cause important stratification in the chamber.

Notation

aTDC *After top dead center.*
bTDC *Before top dead center*
BDC *Bottom dead center*
DI *Direct injection*
DMS *Differential mobility spectrometer*
IMEP *Indicated Mean Effective Pressure*
PN_{ratio} *Ratio between the particle number detected in the 10-23 nm range and the particles detected in the 10-230nm range*
PN_{tot} *Total Particle number*
PN_{10-23} *Particle number detected in the 10-23 nm range*

PF *Port fuel injection*
SOI *Start of injection*
TDC *Top Dead Center*
TMPD *Tetramethyl-p-Phenylenediamine*
T_w *Engine coolant temperature*

Acknowledgements

This work has been founded by the European project Horizon 2020-UPGRADE, ref H2020-GV-02-2016 GA No. 724036. Authors would like to acknowledge Vincent Ricordeau for the fine work performed in operating the engine and setting up the optical diagnostics. Finally, authors thank Prof. Aizawa and Associate Prof. Shawn Kook for the scientific discussions and advices concerning in-cylinder soot sampling.

1 References

1. Sabathil D, Koenigstein A, Schaffner P, Fritzsche J and Doehler A. The influence of DISI engine operating parameters on particle number emissions, SAE Technical Paper, 2011.
2. Close R. Soot particles from GDI engines: Particle alert for direct-injection gasoline cars, https://www.empa.ch/web/s604/soot-particles-from-gdi (2017).
3. Peckham MS, Finch A, Campbell B, Price P and Davies MT. Study of particle number emissions from a turbocharged gasoline direct injection (GDI) engine including data from a fast-response particle size spectrometer, SAE Technical Paper, 2011.
4. Zhang Y, Ghandhi J and Rothamer D. Comparisons of particle size distribution from conventional and advanced compression ignition combustion strategies. *International Journal of Engine Research* 2016: 1468087417721089.
5. European Union No 459/2012 - 715/2007. COMMISSION REGULATION (EU) No 459/2012of 29 May 2012amending Regulation (EC) No 715/2007 of the European Parliament and of the Council and Commission Regulation (EC) No 692/2008 as regards emissions from light passenger and commercial vehicles (Euro 6).
6. Giechaskiel B, Manfredi U and Martini G. Engine exhaust solid sub-23 nm particles: I. Literature survey. *SAE International Journal of Fuels and Lubricants* 2014; 7: 950–964.
7. Leach F, Stone R, Richardson D, et al. Particulate emissions from a highly boosted gasoline direct injection engine. *International Journal of Engine Research* 2018; 19: 347–359.
8. Anderson JO, Thundiyil JG and Stolbach A. Clearing the air: a review of the effects of particulate matter air pollution on human health. *Journal of Medical Toxicology* 2012; 8: 166–175.
9. Otsuki Y, Tochino S, Kondo K and Haruta K. Portable Emissions Measurement System for Solid Particle Number Including Nanoparticles Smaller than 23 nm, SAE Technical Paper, 2017.
10. Jiao Q and Reitz RD. The effect of operating parameters on soot emissions in GDI engines. *SAE International Journal of Engines* 2015; 8: 1322–1333.
11. Francquevillle L de and Pilla G (eds). *Investigation of particle formation processes in a GDI engine in catalyst heating operation*, 2011.
12. Lewis A, Akehurst S, Turner J, et al. Particulate emissions from a highly boosted gasoline direct injection engine. *International Journal of Engine Research* 2018; 19: 347–359.
13. Pilla G and Franqueville L de. Investigation of particle formation mechanisms in GDI engines during transient heating operation. *SIA 2013* 2013.
14. Reavell K, Hands T and Collings N. A Fast Response Particulate Spectrometer for Combustion Aerosols. In: SAE International, 2002.
15. Gaydon A. *The spectroscopy of flames*: Springer Science & Business Media, 2012.

16. Maligne D and Bruneaux G. Time-Resolved Fuel Film Thickness Measurement for Direct Injection SI Engines Using Refractive Index Matching. In: SAE International, 2011.
17. Yang H, Greszik D, Dreier T and Schulz C. Simultaneous measurement of liquid water film thickness and vapor temperature using near-infrared tunable diode laser spectroscopy. *Applied Physics B* 2010; 99: 385–390.
18. Schulz F, Schmidt J and Beyrau F. Development of a sensitive experimental set-up for LIF fuel wall film measurements in a pressure vessel. *Experiments in Fluids* 2015; 56: 98, https://doi.org/10.1007/s00348-015-1971-1 (2015).
19. Schulz C and Sick V. Tracer-LIF diagnostics: quantitative measurement of fuel concentration, temperature and fuel/air ratio in practical combustion systems. *Progress in Energy and Combustion Science* 2005; 31: 75–121, http://www.sciencedirect.com/science/article/pii/S0360128504000619 (2005).
20. Ma X, He X, Wang J-X and Shuai S-J. Design and Optimization of Multi-component Fuel for Fuel Concentration Measurement by Using Tracer PLIF in SI Engine. *SAE Technical Paper* 2010; 2010-01-0344, http://dx.doi.org/10.4271/2010-01-0344 (2010).
21. Itani LM, Bruneaux G, Di Lella A and Schulz C. Two-tracer LIF imaging of preferential evaporation of multi-component gasoline fuel sprays under engine conditions. *Proceedings of the Combustion Institute* 2015; 35: 2915–2922.
22. Moore W, Foster M, Lai M-C, Xie X-B, Zheng Y and Matsumoto A. Charge Motion Benefits of Valve Deactivation to Reduce Fuel Consumption and Emissions in a GDi, VVA Engine. In: SAE International, 2011.
23. Selamet A, Rupal S, He Y and Keller PS. An Experimental Study on the Effect of Intake Primary Runner Blockages on Combustion and Emissions in SI Engines under Part-Load Conditions. In: SAE International, 2004.
24. Dageförde H, Kiefer A, Samenfink W, Wiese W and Kufferath A. Requirements for spray and tip design of a multi-hole injector for DISI engines. *Proceedings of ICLASS, Tainan* 2015.
25. Habchi C. A comprehensive model for liquid film boiling in internal combustion engines. *Oil & Gas Science and Technology–Revue de l'Institut Français du Pétrole* 2010; 65: 331–343.
26. Kook S, Zhang R, Szeto K, Pickett LM and Aizawa T. In-Flame Soot Sampling and Particle Analysis in a Diesel Engine. *SAE Int. J. Fuels Lubr.* 2013; 6: 80–97.